SMAR 2019 – Fifth Conference on Smart Monitoring,
Assessment and Rehabilitation of Civil Structures

SMAR 2019

Axial stiffness of an Fe-SMA during the activation process

Yajiao YANG [1], Matteo BREVEGLIERI [1], Moslem SHAHVERDI [1, 2]

[1] Structural Engineering Laboratory, Empa, Dübendorf, Switzerland

[2] School of civil engineering, University of Tehran, Tehran, Iran

Contact e-mail: Moslem.Shahverdi@empa.ch

ABSTRACT: A shape memory alloy (SMA) is a material which can return into a predefined shape upon heating or unloading after being subjected to deformation. If this reverse process is prevented by a mechanical fixation, stress is developed in the SMA element. The generated stress, typically identified as recovery stress, enables a SMA material to be used as a pre-stressing element for reinforced concrete structures in civil engineering. The process of heating a SMA to a target temperature and cooling it down to room temperature while keeping the strain constant is called activation. The activation simulates what occurs in a SMA used as a pre-stressing element in concrete structures.
A novel iron-based shape memory alloy (Fe-SMA) with the composition of Fe-17Mn-5Si-10Cr-4Ni-1(V, C) (mass %) was designed at Empa. This new Fe-SMA offers promising thermo-mechanical properties since the recovery stress can achieve more than 300 MPa without any additional 'training' process. During the activation process, the developed force between a Fe-SMA element and concrete depends on the axial stiffness of the Fe-SMA strip (k_{SMA}) and the substrate element. The current study investigates the evolution of a variable modulus $E_{SMA}(k)$ during the activation process. The obtained results can be used in analytical and numerical modeling involving the calculation of interaction forces between SMA elements and the substrate structure.

1 INTRODUCTION

In past decades, nickel-titanium shape memory alloys (NiTi-SMAs) played a leading role in the industry because of their good shape memory effect (SME). However, NiTi-SMAs have an inevitable drawback, i.e. they are expensive, which implies that they cannot easily be employed in a large amount as occurs in civil engineering. As an alternative to NiTi-SMAs, Fe-SMAs have attracted more and more attention in recent years due to their lower cost and good mechanical properties.

Fe-SMAs were first discovered by Sato et al. (1982-1984). Since then, there have been plenty of studies regarding the characterization of their mechanical properties and how to improve the SME [Otsuka et al. (1990), Baruj et al. (2002), Liu et al. (2003), Wen et al. (2014) and Peng et al. (2018)]. The mechanism governing the SME of a Fe-SMA is the phase transformation between γ-austenite (fcc: face-centered cubic) and ε-martensite (hcp: hexagonal close-packed structure). The initial state of a Fe-SMA at room temperature is mainly composed of γ-austenite. During deformation, γ-austenite can transform into ε-martensite as stress is applied. The stress-induced ε-martensite can partially transform back to austenite when the material is heated above the austenite start temperature (A_S). The martensite and austenite transformations are

accomplished by forward and reverse movement of Shockley partial dislocations or equivalent stacking faults.

In civil engineering, the recovery stress of a Fe-SMA attracts a lot of attention [Sawaguchi et al. (2006), Czaderski et al. (2014), Cladera et al. (2014), Shahverdi et al. (2016), Michels et al. (2018), Izadi et al (2018) and Strieder et al. (2019)]. In Figure 1, re-plates (Fe-SMAs strips), from company re-fer AG, with a thickness of 1.5 mm, have been used as external pre-stressing elements for the strengthening a reinforced concrete slab [Michels et al. (2018)]. The re-plates were mechanically fastened at both ends with metallic nails.

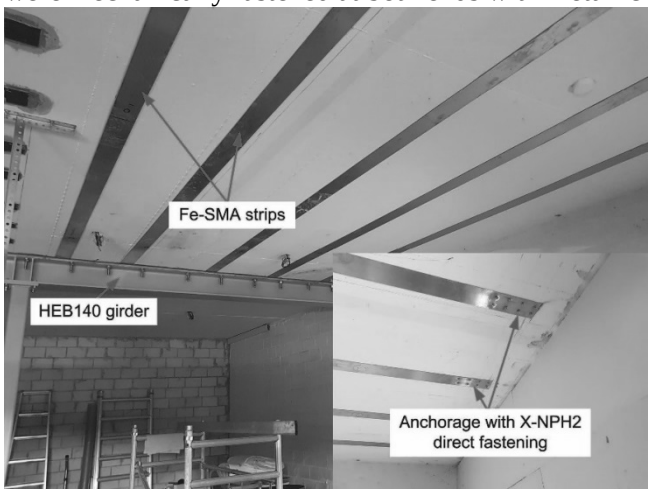

Figure1 Re-plates (Fe-SMA strips) are installed as pre-stressed strengthening elements for a reinforced concrete slab [Michels et al. (2018)]

There are mainly three steps required to achieve recovery stress in civil engineering applications. Step 1: this step is called pre-straining, and consists of reaching the desired strain level in order to generate stress-induced martensite, then releasing the load once the strain level is reached. Step 2: similarly to a conventional steelwork, the SMA strip is fixed at its ends to the concrete (see Figure 1) or alternatively it can be embedded in a shotcrete layer [Shahverdi et al. (2016)]. Step 3: the strip is heated to a target temperature and cooled down to room temperature. This thermal process is called activation. A target temperature of 160 °C is typically chosen since it was observed in Shahverdi et al. (2018) that at this temperature significant recovery stress can be achieved without inducing any damage the concrete.

The activation process consists of 4 stages (see Figure 2): a) Stage I (from room temperature of 23 °C to about 50 °C): the axial stress decreases with increasing temperature due to thermal expansion of the Fe-SMA; b) Stage II (from about 50 °C to 160 °C): the axial stress increases with increasing temperature mainly due to the phase transformation (i.e. the stress-induced martensite transforms back to austenite); c) Stage III (from 160 °C to about 120 °C): the axial stress linearly increases with decreasing temperature mainly because of thermal contraction of the Fe-SMA; d) Stage IV (from about 120 °C to room temperature of 23 °C): the slope of stress-temperature curve starts to change mainly due to phase transformation from austenite to martensite. More details on the recovery stress evolution during the activation can be found in Shahverdi et al. (2018).

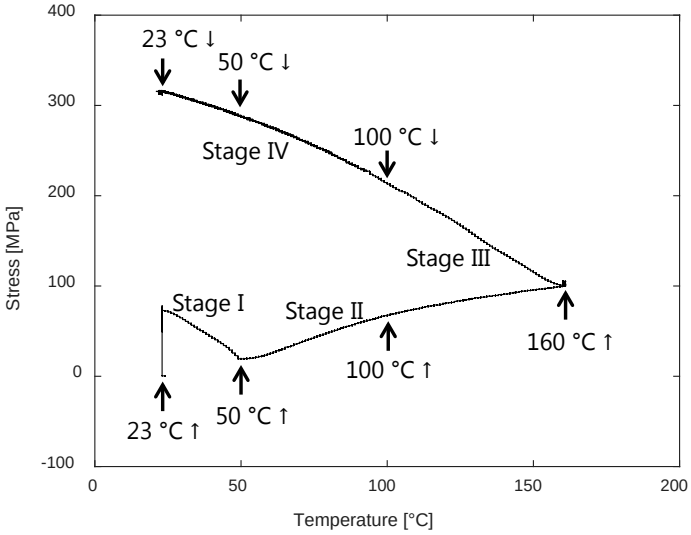

Figure 2 Stress versus temperature curve during the activation process. The Fe-SMA is heated from room temperature to 160 °C and then cooled down to room temperature. The arrows show the target temperatures of the interrupted thermal-mechanical tests (see EXPERIMENTS section).

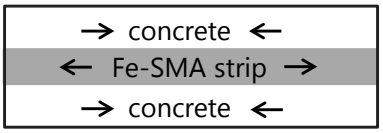

Figure 3 Schematic illustration of the interaction force between the concrete and the Fe-SMA strip (adapted from Lee et al. (2013)).

When SMA strips or bars are embedded or post-installed in the concrete section during the activation process, there is a simultaneous interaction force between the Fe-SMA element and the concrete (see Figure 3). This interaction force can be expressed as a function of α Eq. (1).

$$\alpha = \frac{k_C}{k_{SMA}} \tag{1}$$

Here, k_C and k_{SMA} are the axial stiffness of the concrete and the Fe-SMA element, respectively. The axial stiffness k_{SMA} is calculated as following:

$$k_{SMA} = \frac{AE_{SMA}(k)}{L} \tag{2}$$

A is the cross-section area and L is the length of the tested element. During activation, the value of A and L keeps constant. $E_{SMA}(k)$, however, is a variable that depends on the path of the thermo-mechanical process, indicated here with k. For the virgin material, $E_{SMA}(k)$ is equal to the Young's modulus, $E_{SMA}(k_0)$. During activation, the $E_{SMA}(k)$ cannot be taken as the traditional Young's modulus since the Fe-SMA element is not in the elastic state due to the combined effects of phase transformation and plastic deformations occurring in the material. It is important to investigate how the $E_{SMA}(k)$ develops in order to estimate and model accurately the interaction forces between the different materials [Abouali et al. (2019)]. Among numerous studies about Fe-SMAs, there is no research dedicated to the study of the $E_{SMA}(k)$. This paper aims to investigate the $E_{SMA}(k_0)$ and $E_{SMA}(k)$ of the novel Fe-SMA.

2 EXPERIMENTS

Fe-SMA specimens with length of 250 mm, width of 15 mm and thickness of 1.5 mm were pre-strained to 2% at room temperature by using a 250 kN Zwick machine. The value of pre-straining was chosen based on Shahverdi et al. (2018). The $E_{SMA}(k_0)$ was calculated from the

stress-strain curve during pre-straining phase and was taken as the average value of all specimens (see section 3).

The $E_{SMA}(k)$ was determined by interrupted thermomechanical tests after specimen's pre-straining, which were conducted on a Z020 Zwick machine equipped with a climate-controlled chamber (see Figure 4). The strain was measured by a clip-on Mini MFA 2 extensometer with extension arm (gauge length of the specimen) of 100 mm. At the beginning of the tests, the Fe-SMA specimens were pre-loaded to 50 MPa pre-stress + 10 µm pre-strain (here, the strain is denoted in µm unit, so the actual strain equals to 10 µm divided by extensometer extension arm 100 mm). The preload was applied to avoid compression during constrained heating due to thermal expansion. Then, under strain-control condition, specimens were heated from 23 °C to a target temperature at a thermal rate of 2 °C/min. The target temperatures (shown as black arrows in Figure 2) were 23 °C ↑, 50 °C ↑, 100 °C ↑ and 160 °C ↑ during heating, and 100 °C ↓, 50 °C ↓ and 23 °C ↓ during cooling ('↑' and '↓' indicate if the thermal cycle was interrupted during the heating '↑' or the cooling '↓'). After waiting for one hour at constant target temperature, specimens were loaded to 1% strain at a rate of 0.2 mm/min to determine the $E_{SMA}(k)$. Finally, specimens were cooled down and unloaded. The evolution of parameters (strain, temperature, etc.) was recorded by the textXpertII Software.

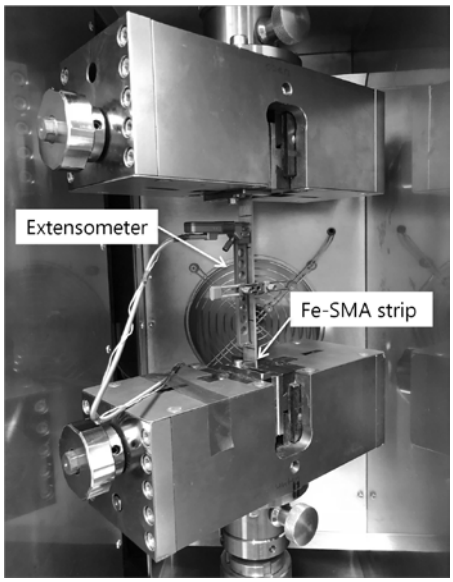

Figure 4 A Z020 Zwick machine equipped with a climate-controlled chamber. The figure shows the inner part of climate chamber: a Fe-SMA strip is fixed in the middle, and the clip-on Mini MFA 2 extensometer is installed on the strip.

3 RESULTS AND DISCUSSION

3.1 Determination of $E_{SMA}(k_0)$

The Young's modulus $E_{SMA}(k_0)$ is determined by fitting with a straight line (regression line) the experimental stress-strain curve in the elastic loading part. Figure 5(a) shows a stress-strain curve during the pre-straining process. The specimen can achieve more than 600 MPa when the strain reaches 2%. Besides, the unloading part deviates from a straight line and this behavior represents the pseudoelasticity phenomenon of Fe-SMAs due to the combination of back transformation from hcp to fcc and a reversible motion of Schockley partial dislocations

according to Leinenbach et al. (2017). In Figure 5(b), the black line depicts the linear fitting in the stress range from 5 to 80 MPa. The average Young's modulus $E_{SMA}(k_0)$, based on 19 tests, is 180 GPa. For each test result, the regression line fits with a R^2 higher than 0.999, which is a goodness-of-fit measure for linear regression models.

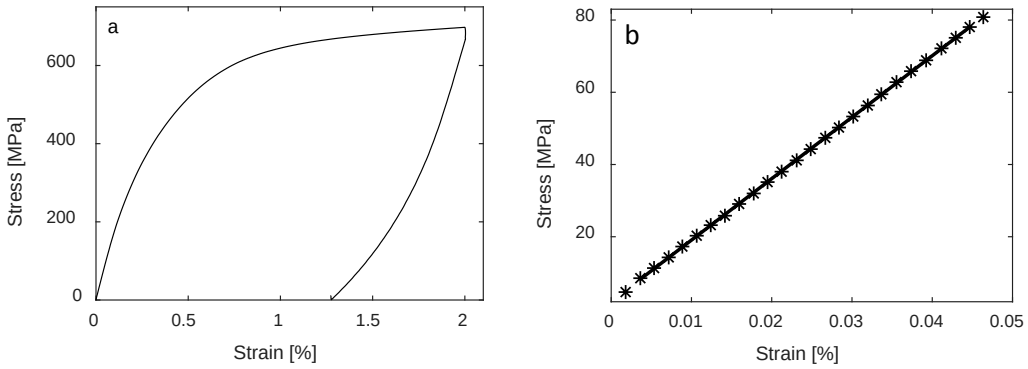

Figure 5(a) Stress as a function of strain during pre-straining to 2%; (b) The black line is linear fitting (regression line) in the stress range from 5 to 80 MPa.

3.2 Determination of $E_{SMA}(k)$

Figure 6(a) shows a pre-straining to 2% and an interrupted thermomechanical test at a temperature of 100°C during the heating phase (100 °C ↑). The $E_{SMA}(k)$ is determined by fitting in the 'pseudo-elastic' loading part of the stress-strain curve with a straight line (regression line). Since the initial axial stress σ_0 at the beginning of loading is not equal to 0, the 'pseudo-elastic' loading part is evaluated in a stress range from σ_0 + 5 MPa to σ_0 + 80 MPa (the value 5 MPa and 80 MPa is the same as the stress range used in section 3.1). In Figure 6 (b), at the beginning of the loading phase, the initial axial stress σ_0 is equal to 71 MPa, which implies that the 'pseudo-elastic' loading part ranges between 76 and 151 MPa. The corresponding calculated $E_{SMA}(k)$ is 201 GPa.

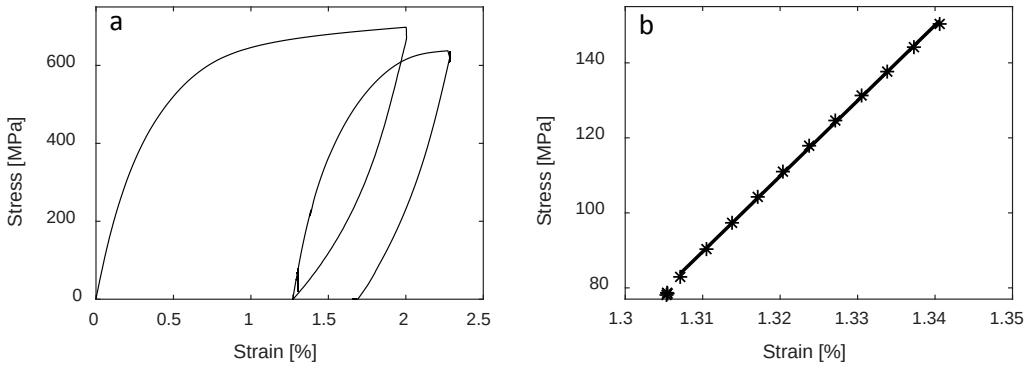

Figure 6(a) (a) Stress as a function of strain during pre-straining to 2% and interrupted thermomechanical test (loading to 1% at 100 °C ↑). (b) The black line is the linear fitting (regression line) in the stress range from σ_0+5 to σ_0+80 MPa.

In comparison, the assessment of the $E_{SMA}(k)$ at 100 °C ↓ can be seen in Figure 7. 100°C ↓ means: heating to 160°C and then cooling to 100°C. As a result, the axial stress σ_0 is 219 MPa,

so the 'pseudo-elastic' loading part ranges between 224 MPa and 299 MPa. The resulting $E_{SMA}(k_0)$ is 155 GPa.

At the same temperature of 100 °C, it is found that there is a difference of 46 GPa in the calculation of the $E_{SMA}(k)$ between heating and cooling phases of the activation.

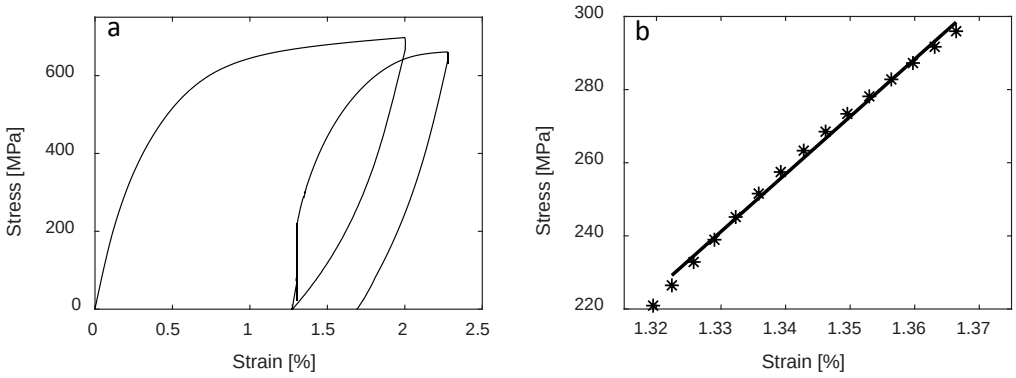

Figure 7 (a) Stress as a function of strain during pre-straining to 2% and interrupted thermomechanical test (loading to 1% at 100 °C ↓). (b) The black line is linear fitting (regression line) in the stress range from σ_0+5 to σ_0+80 MPa.

3.3 The $E_{SMA}(k)$ during the activation process

The final results of the $E_{SMA}(k)$ during activation are presented in Figure 8. At the beginning of the test (23 °C ↑), $E_{SMA}(k)$ is 210 GPa. When the temperature rises up to 50 °C ↑, $E_{SMA}(k)$ slightly increases to 239 GPa. As the temperature further increases, $E_{SMA}(k)$ starts to decrease and reaches 186 GPa at 160 °C ↑. During the cooling process, $E_{SMA}(k)$ keeps decreasing until the thermal cycle is completed (23 °C ↓) and reaches a value of 133 GPa.

During activation, the $E_{SMA}(k)$ is affected mainly by three factors: the microstructure (e.g. martensite and austenite phase fraction), the axial stress and the temperature. During the heating process of activation, some stress-induced martensite can transform back to austenite when the temperature reaches A_s. The austenite phase transformation continues until the temperature reaches austenite finish temperature (A_f). According to Figure 1, the phase transformation induces a transition from stage I to stage II, which indicates that A_s is about 50 °C ↑ in the current test condition. On the other hand, the axial stress increase in stage II demonstrates that A_f is larger than 160 °C ↑. Therefore, the austenite fraction increases with temperature during the heating process. During cooling, the martensite transformation starts when the martensite starting temperature (M_s) reaches (about 120 °C ↓ according to Figure 1). Besides the microstructure, the $E_{SMA}(k)$ evolution during activation is inversely related to the axial stress during activation (The axial stress first decreases and then increases until the end of activation). This reverse correlation indicates that the change of the simultaneous $E_{SMA}(k)$ is mainly due to the axial stress evolution during activation. As for the temperature effect, the $E_{SMA}(k)$ shows a large difference between the tests at the same temperature but with different cooling and heating conditions, e.g. 50 °C ↑ and 50 °C ↓, which indicates that the temperature effect is not a critical factor.

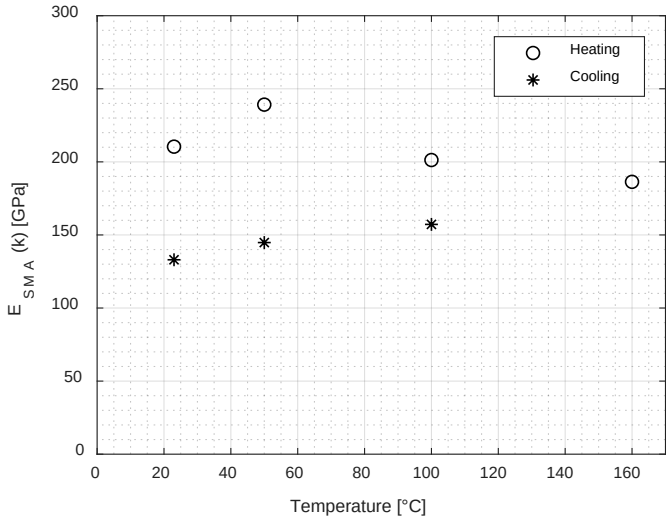

Figure 8 The evolution of $E_{SMA}(k)$ during activation.

4 CONCLUSION AND OUTLOOK

Recovery stress is the main characteristic for Fe-SMAs employed in pre-stressing civil structure; nevertheless, also the stiffness of SMA material plays a relevant role. The results presented in this paper can be used in modeling involving the calculation of interaction forces. The results have clearly shown how the $E_{SMA}(k)$ change during the activation process. In the next step, tests repetitions, as Figure 8, are about to be conducted to calculate average values and error bars. What's more, due to the equipment limitation, the M_s during the cooling process of the activation is still not clear and neither the phase transformation amount (fraction of martensite and austenite) during pre-straining and activation. These mechanisms need more investigation, for example through phase fraction measurement by in-situ X-ray diffraction (XRD).

5 ACKNOWLEDGMENTS

This study was part of a master thesis at Empa. The supply of materials by the company re-fer AG is greatly appreciated.

6 REFERENCES

Abouali, S., Shahverdi, M., Ghassemieh, M. and Motavalli, M. (2019). Nonlinear simulation of reinforced concrete beams retrofitted by near-surface mounted iron-based shape memory alloys. *Engineering Structures*, *187*, 133-148.

Baruj, A., Kikuchi, T., Kajiwara, S. and Shinya, N. (2002). Effect of pre-deformation of austenite on shape memory properties in Fe-Mn-Si-based alloys containing Nb and C. *Materials Transactions*, *43*(3), 585-588.

Cladera, A., Weber, B., Leinenbach, C., Czaderski, C., Shahverdi, M. and Motavalli, M. (2014). Iron-based shape memory alloys for civil engineering structures: An overview. *Construction and building materials*, *63*, 281-293.

Czaderski, C., Shahverdi, M., Brönnimann, R., Leinenbach, C. and Motavalli, M. (2014). Feasibility of iron-based shape memory alloy strips for prestressed strengthening of concrete structures. *Construction and Building Materials*, *56*, 94-105.

Lee, W. J., Weber, B., Feltrin, G., Czaderski, C., Motavalli, M. and Leinenbach, C. (2013). Stress recovery behaviour of an Fe–Mn–Si–Cr–Ni–VC shape memory alloy used for prestressing. Smart Materials and Structures, 22(12), 125037.

Leinenbach, C., Arabi-Hashemi, A., Lee, W. J., Lis, A., Sadegh-Ahmadi, M., Van Petegem, S., and Van Swygenhoven, H. (2017). Characterization of the deformation and phase transformation behavior of VC-free and VC-containing FeMnSi-based shape memory alloys by in situ neutron diffraction. *Materials Science and Engineering: A*, *703*, 314-323.

Liu, D. Z., Kajiwara, S., Kikuchi, T. and Shinya, N. (2003). Atomic force microscopy study on microstructural changes by'training'in Fe-Mn-Si-based shape memory alloys. *Philosophical Magazine*, *83*(25), 2875-2897.

Izadi, M. R., Ghafoori, E., Shahverdi, M., Motavalli, M. and Maalek, S. (2018). Development of an iron-based shape memory alloy (Fe-SMA) strengthening system for steel plates. *Engineering Structures*, *174*, 433-446.

Michels, J., Shahverdi, M. and Czaderski, C. (2018). Flexural strengthening of structural concrete with iron-based shape memory alloy strips. *Structural Concrete*, *19*(3), 876-891.

Michels, J., Shahverdi, M., Czaderski, C. and El-Hacha, R. (2018). Mechanical Performance of Iron-Based Shape-Memory Alloy Ribbed Bars for Concrete Prestressing. *ACI Materials Journal*, *115*(6), 877-886.

Otsuka, H., Yamada, H., Maruyama, T., Tanahashi, H., Matsuda, S. and Murakami, M. (1990). Effects of alloying additions on Fe-Mn-Si shape memory alloys. *ISIJ international*, *30*(8), 674-679.

Peng, H., Wang, G., Wang, S., Chen, J., MacLaren, I. and Wen, Y. (2018). Key criterion for achieving giant recovery strains in polycrystalline Fe-Mn-Si based shape memory alloys. *Materials Science and Engineering: A*, *712*, 37-49.

Sato, A., Chishima, E., Soma, K. and Mori, T. (1982). Shape memory effect in $\gamma \rightleftarrows \epsilon$ transformation in Fe-30Mn-1Si alloy single crystals. *Acta Metallurgica*, *30*(6), 1177-1183.

Sato, A., Soma, K. and Mori, T. (1982). Hardening due to pre-existing ϵ-martensite in an Fe-30Mn-1Si alloy single crystal. *Acta Metallurgica*, *30*(10), 1901-1907.

Sato, A., Chishima, E., Yamaji, Y. and Mori, T. (1984). Orientation and composition dependencies of shape memory effect in Fe-Mn-Si alloys. *Acta Metallurgica*, *32*(4), 539-547.

Sawaguchi, T., Kikuchi, T., Ogawa, K., Kajiwara, S., Ikeo, Y., Kojima, M. and Ogawa, T. (2006). Development of prestressed concrete using Fe–Mn–Si-based shape memory alloys containing NbC. *Materials transactions*, *47*(3), 580-583.

Shahverdi, M., Czaderski, C. and Motavalli, M. (2016). Iron-based shape memory alloys for prestressed near-surface mounted strengthening of reinforced concrete beams. *Construction and Building Materials*, *112*, 28-38.

Shahverdi, M., Czaderski, C., Annen, P and Motavalli, M. (2016). Strengthening of RC beams by iron-based shape memory alloy bars embedded in a shotcrete layer. *Engineering Structures*, *117*, 263-273.

Shahverdi, M., Michels, J., Czaderski, C., and Motavalli, M. (2018). Iron-based shape memory alloy strips for strengthening RC members: Material behavior and characterization. *Construction and Building Materials*, *173*, 586-599.

Strieder, E., Aigner, C., Petautschnig, G., Horn, S., Marcon, M., Schwenn, M. and Bergmeister, K. (2019). Strengthening of Reinforced Concrete Beams with Externally Mounted Sequentially Activated Iron-Based Shape Memory Alloys. *Materials*, *12*(3), 345.

Wen, Y. H., Peng, H. B., Raabe, D., Gutiérrez-Urrutia, I., Chen, J. and Du, Y. Y. (2014). Large recovery strain in Fe-Mn-Si-based shape memory steels obtained by engineering annealing twin boundaries. *Nature communications*, *5*, 4964.